ELSEVIER

Journal of Alloys and Compounds 229 (1995) 158–174

Journal of ALLOYS AND COMPOUNDS

From a molecular view on solids to molecules in solids

Arndt Simon

Max-Planck-Institut für Festkörperforschung, D-70569 Stuttgart, Germany

Received 2 February 1995

Abstract

The structural chemistry of metal-rich compounds formed by metals in groups 1 to 6 is largely based on discrete and condensed clusters. Interstitial atoms play an important role. Structure–property relations are addressed, particularly concerning the interplay of metal–metal bonds and localized magnetic moments as well as superconductivity. Experimental techniques developed for these investigations have been frequently used for low temperature structure research on molecular crystals which is illustrated for HBr, N_2O_3, NO_xCl ($x = 1, 2, 3$), and P_4.

Keywords: Solids; Molecules; Metal-rich compounds; Superconductivity

1. Introduction

When Hugo Fritz Franzen made his invitation to contribute to this special volume of the *Journal of Alloys and Compounds* I was inclined to refuse. The latest review covering the field of our main interest, metal-rich compounds, had just appeared [1] as the latest of many others before [2–12]. No next edition in 1995!

However, I accepted because the aim of this special issue, "to inform students and researchers of the diversity and creativity of modern solid-state chemistry", provides a unique chance not only to show the progress in a specialized field of research, but also to work out how resarch creates new research which sometimes might seem quite unrelated. Research is like a growing tree whose stem becomes larger and clearly structured whilst branches develop from it or new trees from its seed.

In the following certain facets of solid state chemistry will be presented. "Diversity" must be subject to a rather personal view, in our case involving a strong preparative component, theory and concepts, and sufficiently broad elemental variations within such concepts, development of experimental tools. Strong connections within chemistry, e.g. with molecular chemistry, are as essential as with neighboring disciplines such as physics.

2. Metal-rich compounds

The chemistry of metals in low oxidation states is particularly interesting as the residual valence electrons can be used for metal–metal bonding. M–M bonding, although known for many decades, e.g. in Hg_2Cl_2, seemed rather an exception. During the last thirty years research on M–M bonding and metal clusters really exploded, both in solid state as well as in molecular chemistry. It is remarkable how much this kind of chemistry changed our view on regularities in the periodic table. In 1968, a book such as "The Periodic Table" [13] might still have been acceptable as an introduction for students into the chemistry of elements applying only integral oxidation states and omitting the exceptions. The abundance of homonuclear bonding which only accidentally leads to integral oxidation states would forbid such an ordering scheme in our time.

Metal-rich compounds lie between normal valence compounds [14] and the elemental metals with respect to their compositions and frequently with respect to their structures. Although many different metal atom arrangements including interpenetrating icosahedra in, for example, Ta_2S [15] occur, one is not too surprised to find fragments of the usual metal structures, close packing or bcc-type, as essential building units in many structures of metal-rich compounds. A broad structur-

SSDI 0925-8388(95)01681-3

al chemistry can be based on (deformed) M_6 metal octahedra which form the characteristic constituents of discrete or condensed clusters.

Depending on the relative number of ligand atoms, the degree of condensation varies, and oligomeric clusters as well as one-, two- or three-dimensional condensates result. With a sufficient number of valence electrons for M–M bonding the clusters are empty; however, in the case of electron deficiency they need to be stabilized by interstitial atoms. These two aspects, summarized in Fig. 1, serve as guidelines to order and compare such different compound classes as oxides, chalcogenides and halides of group 6 and 5 metals, (carbide, hydride...) halides of group 4 metals and lanthanides, subnitrides of group 2 metals and suboxides of the alkali metals. When progressing through the periodic table in this way, always empty M_6X_8 or M_6X_{12} type clusters, discrete or condensed, are found for the electron-rich group 6 metals. With group 5 metals interstitial atoms in such clusters are rather an exception, however, it is the normal case for the still more electron-deficient group 4 metals and lanthanides. In the subnitrides and suboxides of group 2 and 1 metals, respectively, bare M_6 octahedra centered by nonmetal atoms occur.

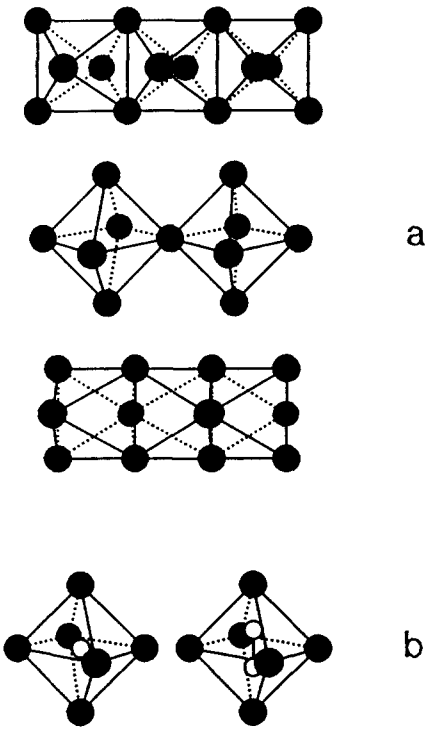

Fig. 1. (a) Condensation of clusters with octahedral M_6 units via (trans-)edges, corners and faces. (b) Interstitial single atoms or molecular groups like C_2 in M_6 octahedra.

2.1. Interstitial atoms in discrete clusters

Molecular orbital calculations [16] provided an early explanation for the experimental fact that 16 (24) electrons can enter M–M bonding states of the M_6X_{12} (M_6X_8) cluster as found e.g. for the ions $Nb_6Cl_{12}^{2+}$ ($Mo_6Cl_8^{4+}$). The closed-shell configuration can also be described in terms of eight three-center bonds into the octahedral faces (12 two-center bonds along the edges) when the ligands lie above the edges (faces) of the M_6 octahedron.

A particularly interesting example of "bond-coloration" has been discovered with the compound $Th_6Br_{15}H_7$. In contrast to the many cases where interstitial atoms occupy central positions in the cluster, the seven hydrogen atoms (statistically) occupy positions 22 pm above the centers of the eight octahedral faces [17,18]. Such $Th_6Br_{12}H_7$ clusters are interconnected via linear halide bridges as in the structure of $Nb_6F_{15} = Nb_6F_{12}F_{6/2}$; see Fig. 2. The electron balance in $Th_6Br_{15}H_7$ formally corresponds exactly to the closed-shell configuration for the M_6X_{12} type cluster ($24 - 15 + 7 = 16$) and the H atoms mark seven centers of the 3-center bonds described for the empty M_6X_{12} type cluster, leaving one 3-center 2-electron M–M bond.

The partial occupation of eight positions by only seven hydrogen atoms raises the question whether the disorder is static or dynamic. Detailed investigations via proton NMR relaxation measurements [19] reveal

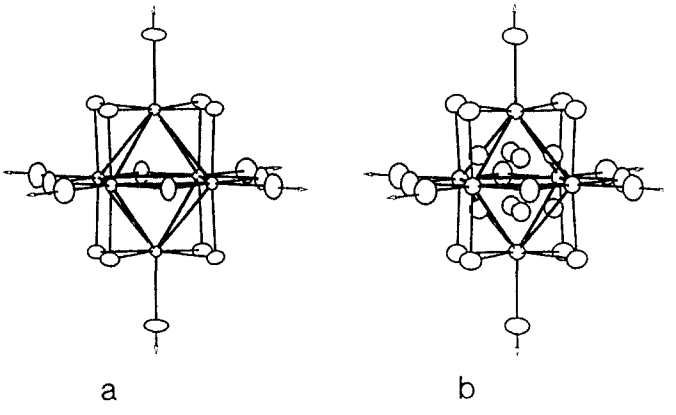

Fig. 2. (a) $Nb_6F_{12}^{i}F_{6/2}^{a,a}$ and (b) $Th_6Br_{12}^{i}H_7Br_{6/2}^{a-a}$ clusters in Nb_6F_{15} and $Th_6Br_{15}H_7$, respectively.

it as being dynamic. A priori, in a cube of hydrogen atoms with one free corner, three kinds of single atom jump are possible (Fig. 3). These could naively be associated with the three regions in a $\ln T_1$ vs. $1/T$ plot

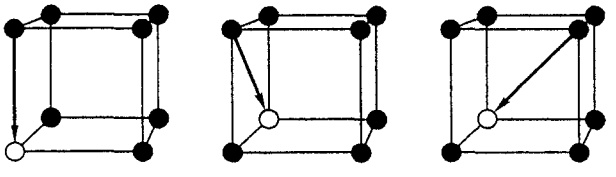

Fig. 3. Different kinds of hydrogen atom motion in the cluster $Th_6Br_{12}H_7$, the hydrogen atoms forming a cube with one vacancy.

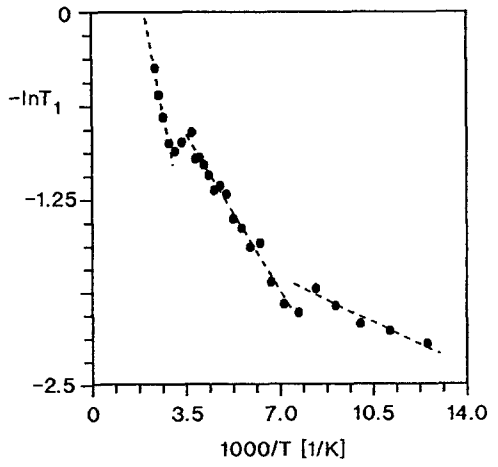

Fig. 4. Arrhenius plot of the longitudinal relaxation times T_1 for $Th_6Br_{15}H_7$.

which exhibits Arrhenius-type behavior (Fig. 4). However, line width measurements show that only the process above 300 K is thermally activated and corresponds to inter-cluster hydrogen diffusion, whereas the positional changes at lower temperature persisting down to 80 K are due to tunneling processes.

Chemical bonding in $Th_6Br_{15}H_7$ is of interest for several reasons. From a special point of view this interest arises from the fact that — according to (relativistic) Extended Hückel calculations [19] — the 5f electrons participate significantly in M–M bonding, in contrast to the 4f electrons in metal-rich lanthanide compounds. From a more general point of view the peculiar role of the interstitial atoms should be mentioned. The bonding of the hydrogen atoms in $Th_6Br_{15}H_7$ is rather ionic. The hydrogen-like bands are below in energy of the bands with bromine character. Hence, the "stabilization" of the cluster by the interstitial atoms is due to removing weak M–M bonding and creating strong heteropolar bonds between M atoms and interstitials. In the case of $Th_6Br_{15}H_7$ still two metal-centered electrons are present for M–M bonding. However, in the case of the $Gd_{10}Cl_{18}(C_2)_2$ entity formed from edge condensation of two $Gd_6Cl_{12}C_2$ units all valence electrons are removed from the metal atoms according to $(Gd^{3+})_{10}(Cl^-)_{18}(C_2^{6-})_2$. The compound is an ethanide chloride ($d_{c-c} \approx 145$ pm), in spite of the cluster topology of the $Gd_{10}Cl_{18}$ entity which is essentially the same in a strongly M–M bonded cluster of the more electron-rich metal molybdenum in the compounds $La_2Mo_{10}O_{16}$ and $Pb_2Mo_{10}O_{16}$ [20,21]. Actually, the borderline between simple salts and real cluster compounds is crossed with these examples.

2.2. Cluster condensation

The analysis of a large body of crystal structures of metal-rich compounds between transition metals and p elements led to the concept of cluster condensation [8]. In spite of the inherent weakness that this qualitative concept is based on topology and focusses on the metal atom arrangement with only a second-order contribution to chemical bonding, the concept proved to be extremely helpful in suggesting new chemistry, e.g. in transition metal oxides. The state of the art is presented in [1] and should not be repeated here. However, it is tempting to cast light on two aspects, namely the tremendous chemical complexity of such condensed cluster systems on the one hand and the degree of understanding of such complexity on the other.

The last section ended with the introduction of the $Mo_{10}O_{18}$ cluster formed from two Mo_6O_{12} clusters joined via a common edge of the Mo_6 octahedra with the loss of those oxygen atoms above the edge involved in condensation. The $Mo_{10}O_{18}$ cluster represents the first step of condensation via trans-edges of the Mo_6 octahedron which ends in the infinite Mo_4O_6 chain, e.g. in the compound $NaMo_4O_6$ [22]. This chain is the basic building unit in numerous reduced oxomolybdates [23]. Fragments of this chain, "oligomeric" clusters formed from 2 to 5 condensed Mo_6 octahedra, exist in phases which are prepared under slightly oxidizing conditions compared to the infinite chain compounds by using e.g. quartz glass ampoules instead of capsules of molybdenum. Magic electron numbers for certain oligomer sizes can only be estimated roughly due to the fact that cluster distortions and variable inter-cluster contacts adjust for differing electron concentrations.

Another problem adds to the difficulty in preparing pure phase samples and leads to epitaxial intergrowth of layers formed from different oligomers. The phases $In_5Mo_{18}O_{28}$, $In_{11}Mo_{40}O_{62}$ and $In_3Mo_{11}O_{17}$ contain layers of $(Mo_6)_4$, $(Mo_6)_4+(Mo_6)_5$ and $(Mo_6)_5$ units, respectively. These phases could be characterized by single-crystal X-ray analysis [24–26]; however, being aware of the marginal differences in composition of $In_{1.11}Mo_4O_{6.22}$, $In_{1.10}Mo_4O_{6.20}$ and $In_{1.09}Mo_4O_{6.18}$, one expects severe disorder, as indeed is obvious from the high resolution electron micrograph of a crystal fragment of $In_5Mo_{18}O_{28}$ presented in Fig. 5 [27]. The image shows intergrowth of different oligomer layers which results in a one-dimensional disorder. In addition, changes in the stacking sequence are observed and these lead to monoclinic and orthorhombic symmetry if long range ordered. Actually, the stacking of three oligomer layers offers four different possibilities. So far the above-mentioned two are the only ones observed. These rather sketchy remarks may give some feeling for the complexity of a field where the definition of a phase in a thermodynamic sense reaches its limits.

An even more complicated intergrowth is found in the phasoid [28] prepared in the Ba–Nb–O system

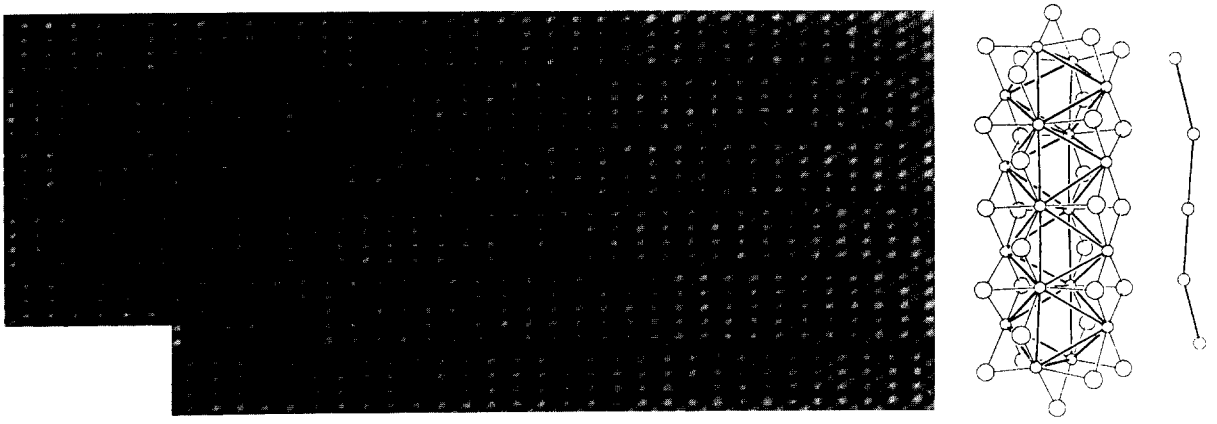

Fig. 5. (left) HRTEM image of $In_5Mo_{18}O_{28}$ in [010] direction. The single slab is composed of (right) linear In_5^{7+} cations and $(Mo_{18}O_{26}O_{4/2})^{7-}$ anions formed by condensation of four Mo_6 units. A fault is shown with the second slab from the bottom which contains clusters of five Mo_6 units and In_6 cations.

[29]. The HREM image (Fig. 6) shows an irregular intergrowth of fractions of the NbO structure — dark crosses represent Nb_6 octahedra condensed via corners and projected along the (pseudo-)fourfold axis — and perovskite type $BaNbO_3$. The different kinds of fragments give some indication of the large number of (ordered) phases which possibly exist in the system if a regular intergrowth can be achieved. So far, ordered compounds based on the clusters and cluster condensates shown in Fig. 7 are known from different sources (see references in Refs. [2,30]).

In the NbO type fragments the Nb_6O_{12} clusters are complete (in contrast to the clusters in oxomolybdates discussed above). This fact helps in working out a rule to derive the optimal electron concentrations for different types of fragments. Fig. 8 illustrates the underlying procedure. In NbO the niobium is left with three electrons for M–M bonding, which is just appropriate to avoid filling band states with dominating Nb–O antibonding interaction. The discrete Nb_6O_{12} cluster as it occurs e.g. in $Mg_3Nb_6O_{11}$ [31] calls for 14 electrons (2.33 per Nb atom). The closed-shell configuration with 16 electrons is avoided, as the strong antibonding Nb–O interactions make the highest lying M–M bonding orbital effectively antibonding. The $Nb_{11}O_{20}$ cluster in $K_4Al_2Nb_{11}O_{20}F$ [32] has 24 electrons in M–M and overall bonding orbitals. This cluster contains a central niobium atom bonded as in NbO ($3e^-$) and two atoms at the ends bonded as in the Nb_6O_{12} cluster ($2.33e^-$), which leaves approximately 2 electrons for the rest of 8 niobium atoms to make a sum near 24.

It is sufficient to differentiate the niobium atoms in a NbO fragment structure according to these three functionalities to derive the optimized electron count for the fragment. To illustrate the procedure, the compound $BaNb_7O_9$ might be chosen as an example [33]. As Fig. 9 shows, slabs of the NbO structure containing twin layers of corner-sharing Nb_6 octahedra alternate with BaO layers. Per formula unit five Nb atoms are surrounded as in NbO ($3e^-$) and two are neighbors to them ($2e^-$). The calculated electron

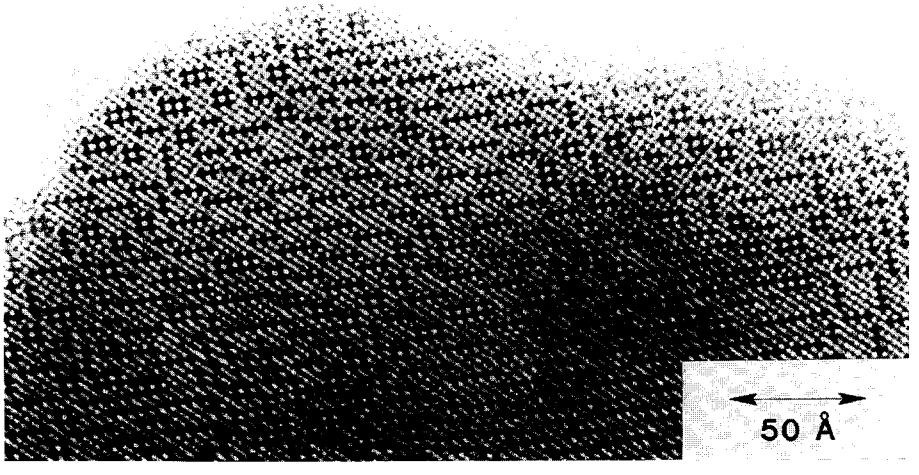

Fig. 6. HRTEM image of the Ba–Nb–O phasoid [29].

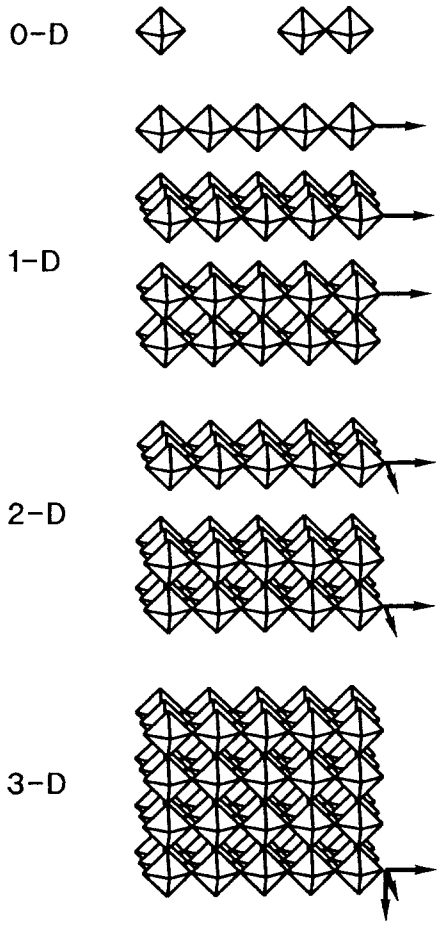

Fig. 7. Schematic representation of the increasing dimensionality of condensed cluster frameworks in reduced oxoniobates with single Nb_6O_{12} clusters, e.g. in $Mg_3Nb_6O_{11}$, twin octahedra in $K_4Al_2Nb_{11}O_{21}$, chains in $BaNb_5O_8$, triple chains in $Ba_4Nb_{14}O_{23}$, layers in $BaNb_4O_6$, twin layers in $BaNb_7O_9$ and 3-dimensional framework in NbO.

number for M–M bonding in the Nb_7O_8 slab is therefore 19, in perfect agreement with the number derived via the ionic limit for the actual compound, $Ba^{2+}(Nb^{5+})_7(O^{2-})_9 \cdot (e^-)_{19}$.

Such good agreement also holds for the other known phases summarized in Fig. 7. Developing the rich structural chemistry of NbO type fragments promised by the image of the phasoid (Fig. 6) apparently only fills gaps in a system that is well established already. However, there might be other challenges to go on. Special interest in such reduced oxoniobates could arise from recent findings that phases in the Ba–Nb–O system of yet unknown composition show superconductivity above 20 K [34].

2.3. Condensed cluster structures with interstitials

Proceeding to metal-rich halides of the rare earths metals, a very rich chemistry of condensed cluster phases is found. Due to the valence electron poor

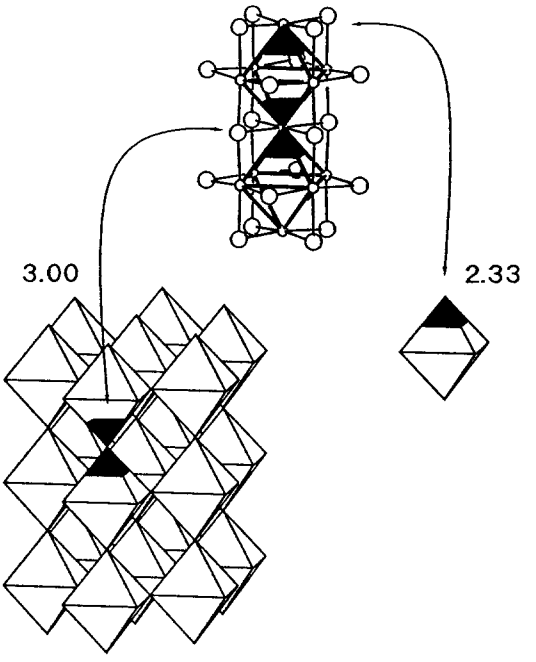

Fig. 8. Derivation of the valence electron counting scheme for M_6X_{12}-type clusters condensed via apex atoms of the M_6 unit. Three electrons are associated with M atoms surrounded as in NbO, 2.33 electrons for atoms surrounded as in the discrete M_6X_{12} cluster.

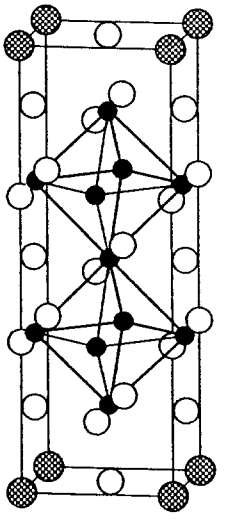

Fig. 9. Tetragonal unit cell of $BaNb_7O_9$ (filled, hatched and empty circles for Nb, Ba and O, respectively) exhibiting twin layers of condensed Nb_6O_{12} clusters as characteristic fragments of the NbO structure.

nature of these metals the cluster frameworks contain interstitial atoms with only very few exceptions like Gd_2Cl_3 [35,36]. Indeed, this chemistry lies at the borderline to simple salts with no M–M bonding and there are numerous cases where this borderline is easily crossed.

In opening a new field, preparative techniques need to be developed. In the case of metal-rich lanthanide

compounds the use of arc-welded tantalum containers proved essential [37] to avoid reactions with oxygen from ceramics or glass. A survey of existing compounds and structural features of these compounds was presented in Ref. [4]. In the meantime the knowledge has broadened, including new cluster types like the C_2 centered trigonal bipyramidal Pr_5C_2 unit [38]. In particular, compounds containing different kinds of interstitials simultaneously became known. Carbide hydride halides [39], carbide oxide halides [40,41], carbide nitride halides [42] and carbide boride halides [43] of increasing structural complexity have been found. Instead of going into any detail with these new chemical and structural results it is tempting to address the aspect of structure property relations. Investigations in this direction are interesting for several reasons. Metal-rich rare earth metal compounds offer a unique possibility to study the interplay of M–M bonding with localized magnetic moments. The specific geometrical conditions of condensed cluster systems lead to pronounced dimensionality as well as frustration effects. Last but not least, the competition between localization and delocalization of electrons makes certain phases a kind of model compound to study the phenomena of superconductivity. Examples of each of these aspects are presented in the following sections.

2.3.1. Properties of $Gd_2XC(H)$

The phases Gd_2XC (X = Cl, Br, I) have one electron per formula unit in excess of a normal valence compound according to the ionic formulation $(Gd^{3+})_2X^-C^{4-}e^-$, and this electron is involved in M–M bonding. This crude view of chemical bonding can easily be verified by band structure calculations; however, a simple experimental proof is also possible. The electrons delocalized in a conduction band with M–M bonding character can be "titrated" with hydrogen. By heating the compounds at 820 K in hydrogen, a topochemical reaction leads to the formation of Gd_2XCH [39]. As discussed earlier for $Th_6Br_{15}H_7$, each hydrogen atom localizes an electron by forming the hydride anion H^-, and at the given composition the M–M bonding conduction band has changed into a low-lying band with mainly hydrogen character. The change is clearly seen in the electrical properties which are metallic for e.g. Gd_2BrC but semiconducting for Gd_2BrCH (Fig. 10(a)). The structural change as seen in neutron diffraction investigations on the deuterated iodides is small (Fig. 10(b)). The deuterium atoms slip into the layers of edge-condensed, C centered Gd_6 octahedra and occupy positions above triangular faces very much like in the case of the discrete cluster $Th_6Br_{12}H_7$.

The comparison of the resistance curves for Gd_2BrC and Gd_2BrCH, respectively, reveals characteristic features beyond mere differences in magnitude. Whereas Gd_2BrCH exhibits a smooth increase of the resistance to low temperature, the curve for Gd_2BrC shows an abrupt change in slope. The sudden decrease of the resistance is caused by a transition into a magnetically ordered state accompanied by reduced (magnetic) disorder scattering. Whereas the non-conducting Gd_2BrCH does not order in the observed temperature range, the delocalized M–M bonds in Gd_2BrC open a "channel of information" between the magnetic moments of the Gd $4f^7$ cores which drives the ordering temperature to above 100 K. This enhanced interaction between localized moments via a polarization of the electron gas in metals is well known as the RKKY interaction. Elemental gadolinium orders ferromagnetically near room temperature; the salt $GdCl_3$ does it below liquid helium temperature. However, as we see in the next section, not only conduction electrons provide this additional coupling mechanism between the magnetic moments of the cores, but also localized M–M bonds.

To complete the story, the detailed investigation of the ordering processes in Gd_2XC leads to the result that the chloride is an antiferromagnet, whereas bromide and iodide order ferromagnetically [44] (Fig. 11). This different behavior is clearly related to the differ-

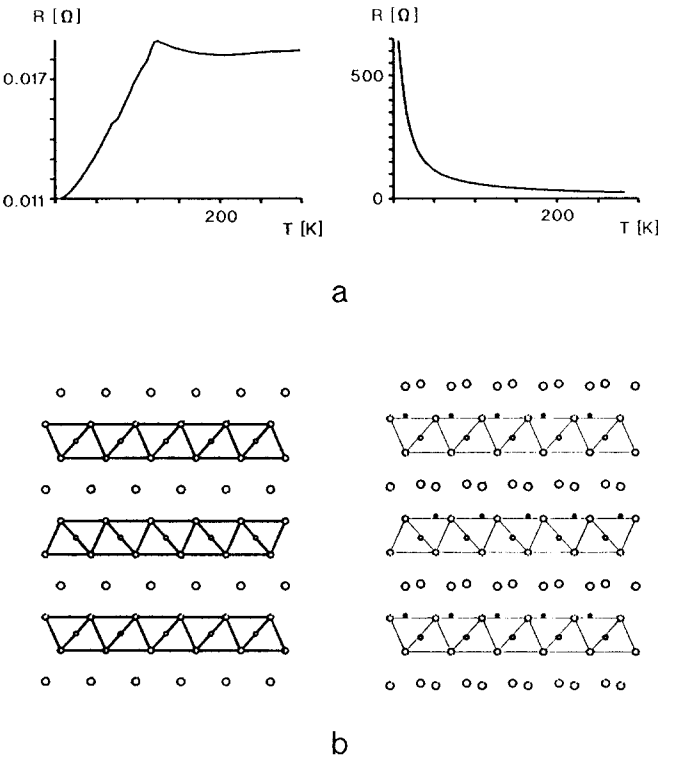

Fig. 10. (a) Electrical resistance of metallic Gd_2BrC (left) and semiconducting Gd_2BrCH (right). (b) Crystal structures of Gd_2IC (left) and Gd_2ICD (right) as determined by neutron diffraction. The loss of M–M bonding in Gd_2ICD is indicated by weak lines between the Gd atoms.

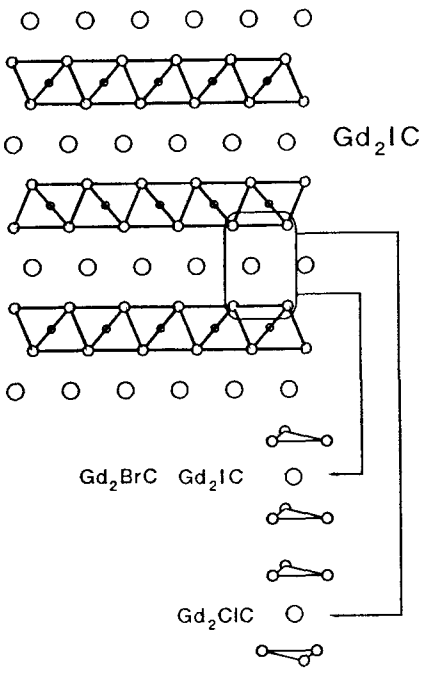

Fig. 11. Crystal structures of Gd_2XC. The coordination polyhedron is a trigonal prism around X = Br,I and a trigonal antiprism around X = Cl leading to ferromagnetic and antiferromagnetic coupling, respectively.

ent halogen atom coordinations. The coordination of the chlorine atom is trigonal antiprismatic and hence the linear M–Cl–M bridge favors antiferromagnetic coupling. In contrast, the M–(Br,I)–M bridge is bent due to the trigonal prismatic coordination favoring ferromagnetic coupling.

2.3.2. Dimensionality and frustration effects in Gd_2Cl_3

Gd_2Cl_3 forms black needles whose crystal structure [35,36] is shown in Fig. 12. Chains of trans-edge sharing octahedra, strongly elongated in chain direction, are well separated by chlorine atoms between them.

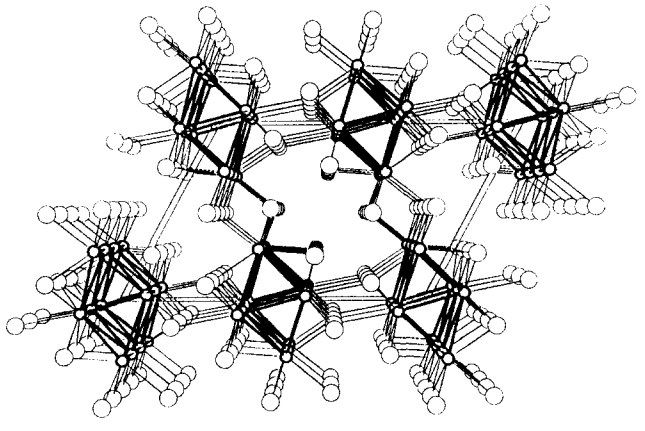

Fig. 12. Crystal structure of Gd_2Cl_3 projected along the monoclinic *b* axis. The chains of (trans-)edge sharing Gd_6 octahedra are enhanced by bold lines.

In spite of close M–M contacts and a non-integer number of excess electrons per gadolinium atom, Gd_2Cl_3 is a semiconductor with a band gap of 0.85 eV [45]. It orders antiferromagnetically at 26.8 K. This temperature is again an order of magnitude higher than for the salt $GdCl_3$, where the coupling mechanism is restricted to dipolar interactions between the gadolinium ions. The magnetic behavior of Gd_2Cl_3 shows clearly that the f electrons can also effectively be coupled via localized M–M bonds involving d electrons.

Studies of the ordering process with specific heat and neutron diffraction measurements [4] are full of surprises. At the beginning the tiny peak in the specific heat curve for Gd_2Cl_3 was overlooked. One would expect a pronounced heat effect when the configurational entropy due to ordering of the large moments of $S = 7/2$ ions is lost. Comparison with the mass-normalized specific heat of nonmagnetic Y_2Cl_3 indicates [4] a very significant contribution to the specific heat which is of magnetic origin and is due to fluctuations in the one-dimensional system (Fig. 13). The magnetic part of the specific heat can be modelled by a Heisenberg chain with $S = 7/2$ and an exchange constant $J = -2.6$ K [4]. The onset of three-dimensional magnetic order at 26.8 K is proven by the appearance of superstructure reflections in a neutron diffraction experiment on a single crystal of Gd_2Cl_3 which call for a doubling of the *c*-axis length and (magnetic) non-equivalence of neighboring chains. The order of moments within a chain at 14.5 K is shown in Fig. 14.

The atoms in the octahedra bases form two ferromagnetic chains with moments parallel to the chain

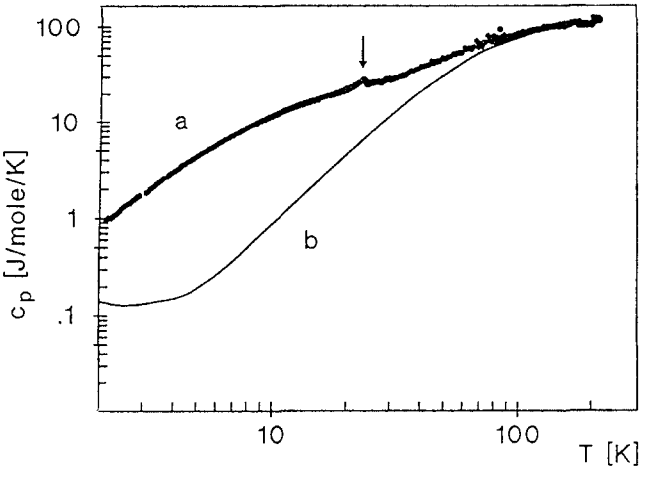

Fig. 13. Specific heat measurement for (a) Gd_2Cl_3. The arrow marks the tiny excess heat at the magnetic ordering transition. For comparison the (mass-normalized) specific heat for (non-magnetic) Y_2Cl_3 is shown (b). The excess heat of Gd_2Cl_3 is due to one-dimensional magnetic fluctuations in the chains.

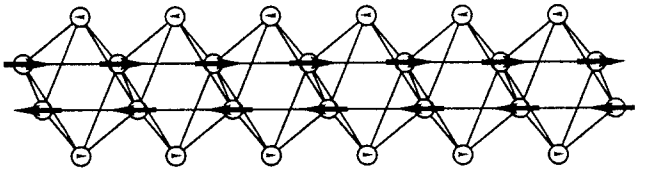

Fig. 14. Magnetic order within the chains of Gd_2Cl_3. The moments in the octahedra bases are ordered, whereas the moments on the apex atoms are disordered owing to frustration.

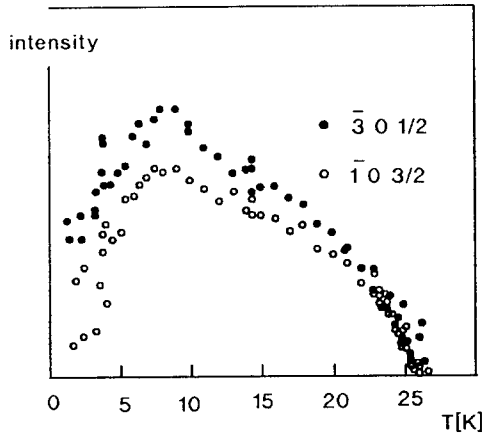

Fig. 15. Magnetic superstructure reflections as a function of temperature in the neutron diffraction diagram of Gd_2Cl_3.

axis which then are antiferromagnetically coupled. A large moment, 5.5 μ_B instead of the theoretical value 7 μ_B, is found on these atoms. In contrast, the moment on the apex atoms is much smaller, approximately 1 μ_B. It is obvious that this effect is due to a frustration problem. In the triangular octahedral face two moments are ordered antiparallel — the short M–M bond provides strong antiferromagnetic coupling — and the third is frustrated, so it stays essentially disordered.

When the neutron diffraction experiments were extended to temperatures well below 14.5 K, the intensities of the magnetic superstructure reflections did not level off at the lowest temperatures as expected but decreased again after passing a maximum around 7 K [46]; see Fig. 15. This not yet quantitatively understood effect is one more surprise which shows that questions raise experiments and the results raise new questions. But this is a well known fact.

2.3.3. Superconductivity in $RE_2X_2C_2$ phases

When discussing hydrogen atoms as interstitials, e.g. with $Th_6Br_{15}H_7$ or Gd_2XCH, it was argued that these atoms played the role of electron acceptors without too much of a covalent interaction with the host lattice. In the last example chosen such interactions play an important role.

The structures of the phases $RE_2X_2C_2$ shown in Fig.

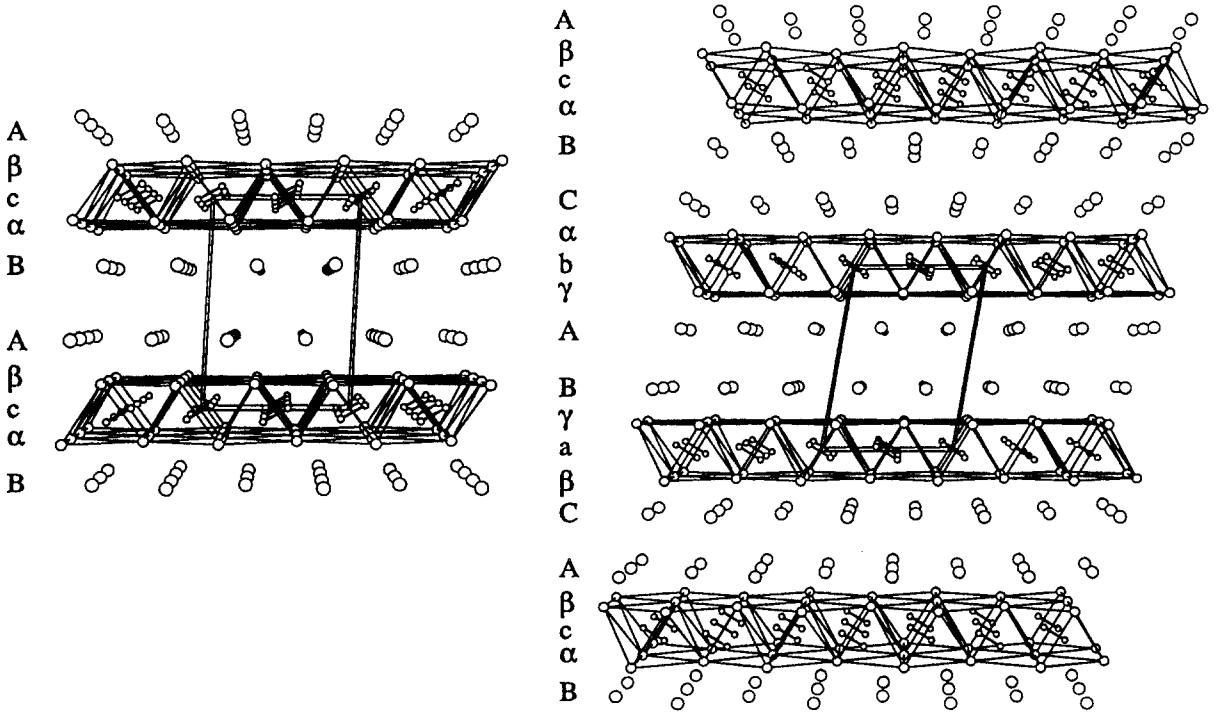

Fig. 16. Stacking variants 1s and 3s in $Y_2X_2C_2$ phases (X, Y, C atoms drawn with decreasing sizes). The stacking sequences are indicated and the unit cells are outlined.

16 are closely related to that of Gd_2XC. The main difference lies in the fact that the doubled halogen content creates van-der-Waals gaps between the layers of condensed M_6 octahedra. Another difference is due to the substitution of single C atoms by C_2 units. Both Gd_2CX and $RE_2X_2C_2$ are metallic, the latter having a two-dimensional metallic character, yet the origin of the metallic conductivity is entirely different in both cases. While Gd_2XC is a "true" metal because an excess of valence electrons partially fills the conduction band which has an essentially M–M bonding character as discussed earlier, the phases RE_2X_2C are metals "by accident".

As visualized by a simple molecular orbital scheme for the C_2 unit in $RE_2X_2C_2$ (see Fig. 17), these compounds must be addressed as ethenide halides corresponding to the ionic formulation $(RE^{3+})_2(X^-)_2C_2^{4-}$ in agreement with the observed short distance $d_{c-c} \approx 130$ pm. The electronic delocalization is therefore due to back bonding from the highest occupied π^* orbital of the C_2 unit into empty d states of the surrounding metal atoms. It is interesting to note that such d–p interaction frequently discussed in molecules manifests itself directly in the metallic property of $RE_2X_2C_2$. In the case of nonmagnetic RE metals superconductivity was found [49]. Fig. 18 shows resistivity, Meissner effect and shielding measurements for the transition in $Y_2Br_2C_2$. The transition temperature is low; however, the compound nicely models ideas about the chemical origin of superconductivity that we have followed for a number of years [50–54].

Instead of single electrons in a normal metal, paired electrons are the charge carriers in a superconductor. By the way, there is a long-standing debate about the possibility or realization of one-step two-electron charge transfer in chemistry [55,56]. As a final argument it is heard that what looks like a simultaneous transfer of two electrons in a measurement might resolve into a two-step process in measurements with different time windows. Paying attention to the collective behavior in a solid might be helpful in this debate, as the one-step two-electron charge transfer is well established between superconductors coupled via a Josephson barrier.

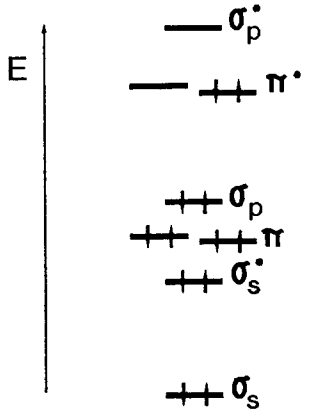

Fig. 17. Schematic MO diagram (arbitrary energy scale) for the C_2^{4-} ion in $RE_2X_2C_2$. The removal of orbital degeneracy is due to the monoclinic symmetry of the structure type.

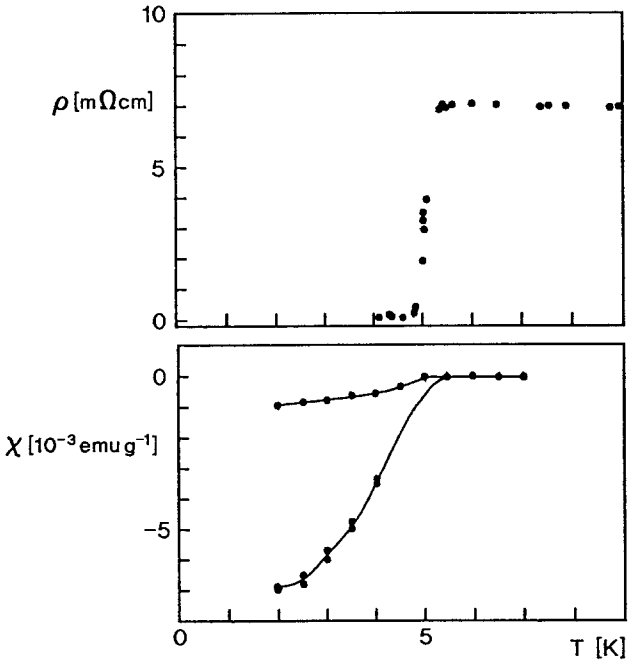

Fig. 18. Superconducting transition of $Y_2Br_2C_2$ indicated by the (top) resistivity drop and (bottom) Meissner and shielding effect.

According to BCS theory, electron–phonon interaction is the origin for the coupling of conduction electrons leading to Cooper pairs which are characterized by opposite spin and momentum for every two electrons involved $\{\vec{p}\uparrow, -\vec{p}\downarrow\}$. Electron–phonon coupling also plays an essential role in high-T_c superconductivity [57].

It is shown that attractive interactions between conduction electrons always lead to superconductivity [58] (if no localization in a distorted lattice occurs). In order to gain a chemical understanding of the phenomenon of superconductivity, an answer is needed to the question of how a specific arrangement of certain atoms leads to an attraction between equally charged carriers, electrons or holes. Real space arguments are needed.

Formally, the description of a Cooper pair, $\{\vec{p}\uparrow, \vec{p}\downarrow\}$ reminds one of a localized electron pair, e.g. in a chemical bond which is spin paired and has net momentum zero. A pairwise attractive interaction between conduction electrons thus may translate into a situation near pairwise localization of electrons.

Dynamic changes of the lattice geometry, phonons, strongly influence this tendency towards localization (electron–phonon coupling).

The special bonding in $RE_2X_2C_2$ may be used to illustrate this idea. In agreement with the qualitative conclusions from the MO scheme (Fig. 17) the band structure calculation performed on $Gd_2Cl_2C_2$ [59] shows a nonzero density of states (DOS) at the Fermi level, due to mixing of $C_2\pi^*$ and Gd d_{t2g} states; see Fig. 19. Very small dispersion of bands at the Fermi level in certain directions of the zone [59,60] indicates a tendency towards electronic localization. It can be concluded that $RE_2X_2C_2$ phases are metallic owing to RE–C covalency with a tendency to pairwise localize electrons in the (quasi molecular) π^* orbitals of the C_2 units. The stretching vibration of the C_2 unit will couple to the conduction electrons via a (dynamic) change of the energy the π^* orbital relative to the Fermi level, as will a wagging vibration of the C_2 unit which influences the RE–C covalency. Phonons provide a long-distance coherence for the pairing electrons. A generalization of the idea involves antibonding states close to the Fermi level (e.g. $Cud_{x^2-y^2}$ in oxocuprates), nonbonding states (e.g. lone pair in oxobismutates) or bonding states (e.g. M–M bonds in A15 compounds or suppressed charge density waves in Nb, Ta dichalcogenide phases).

The layered compounds $RE_2X_2C_2$ offer interesting possibilities to study the idea experimentally. (i) The covalent RE–C bonding can be changed by varying the RE_6 octahedron around the C_2 unit via X atom replacement. (ii) Intercalation reactions with donors or acceptors will change the position of the Fermi level relative to the $C_2\pi^*$ level. First results [61] concerning (i) are presented in Fig. 20 for the phases $Y_2(Cl,Br,I)_2C_2$. A gradual substitution of Cl by the larger Br atom and of Br by the larger I atom results

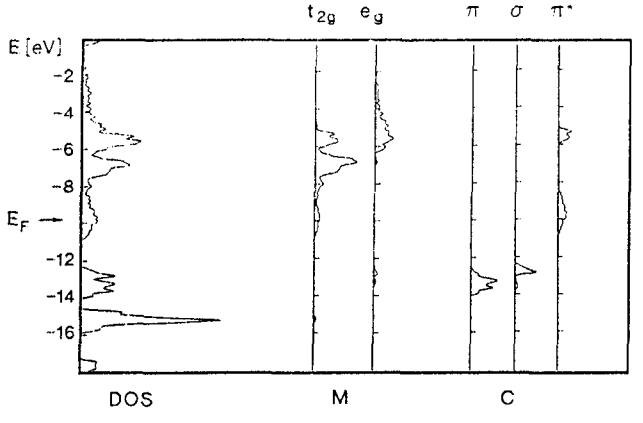

Fig. 19. Band structure for $RE_2X_2C_2$ performed for RE = Gd. From left to right: total density of states (DOS), projected densities for metal (M) and carbon (C).

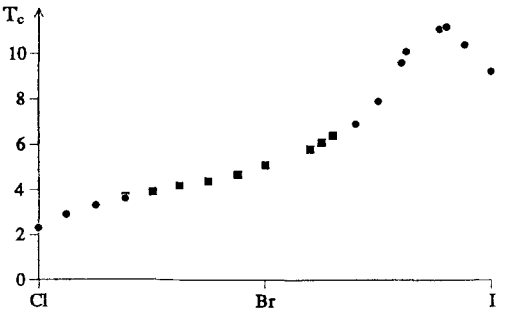

Fig. 20. Superconducting transition temperatures T_c of $Y_2X_2C_2$ (X = Cl, Br, I) as a function of composition. Circles and squares denote 1s and 3s stacking variants, respectively.

in a smooth increase of the a lattice constants (in plane distances) accompanied by a gradual increase of T_c.

The transition temperature has a maximum $T_c \approx 11$ K at a composition $Y_2Br_{0.5}I_{1.5}C_2$ indicating an optimization of the metrics with respect to T_c for this system. Structural changes from 1s to 3s form occur at a composition near $Y_2Cl_{1.2}Br_{0.8}C_2$ and back to 1s near $Y_2Br_{1.2}I_{0.8}C_2$. These changes are not reflected in the transition temperatures in spite of discontinuities observed for the interplane distances. Clearly, the coupling mechanism has to be sought in a single $Y_2X_2C_2$ slab.

Intercalation experiments (ii) have not been performed yet. Concerning the optimized adjustment of the Fermi level to the $C_2\pi^*$ level, which is the idea behind these experiments, an analysis of a closely related compound class, rare earth carbides, must be mentioned. Superconductivity in these phases was the subject of numerous investigations [62]. Inspection of the published data shows that superconductivity is found only for those phases which contain C_2 units. Partial substitution of the metals by others created a large body of materials with varying valence electron concentration. One can refer to a composition $RE_xM_yC_2$ and calculate the number of electrons transferred to two carbon atoms assuming a transfer of all valence electrons of the electropositive metals as in the ionic limit for $RE_2X_2C_2$. Fig. 21 shows a plot of T_c as a function of the number of transferred electrons for $Y_xM_yC_2$ phases formed with yttrium and M = Ti, Zr, Th. The number of electrons is sufficiently low for a persistance of C_2 units, and it is obvious from Fig. 21 that the optimal band filling for superconductivity occurs with four (or slightly more than four) electrons to allow for an occupation of the π^* orbital in a double-bonded "C_2^{4-}" entity as for $RE_2X_2C_2$. A similar plot on the basis of all known rare earth carbides verifies this finding [63]. The formal similarity of such a plot with a Matthias plot [64] raises the question whether a second maximum in T_c can be

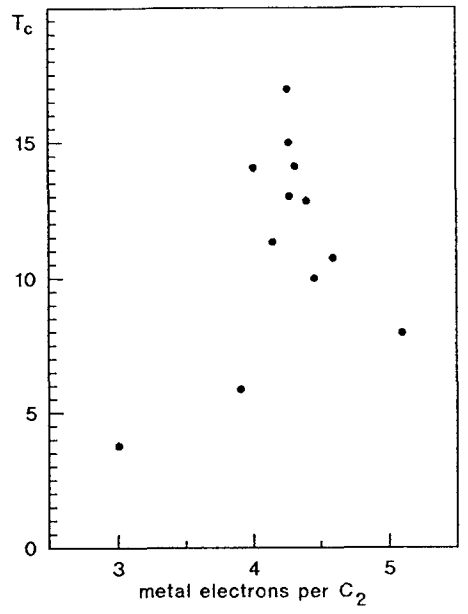

Fig. 21. Superconducting transition temperature T_c as a function of electron concentration for binary and ternary yttrium carbides. A maximum value is given for a sample of composition $Y_{0.90}Th_{0.39}C_2$.

reached at a band filling that allows a transfer of 6 electrons per C_2 unit.

2.4. Bare metal clusters in solids

Metal–metal bonding, if it occurs in compounds of the alkali and alkaline earth metals, must be special because of the low valence electron number of these metals. Discrete and condensed octahedral clusters formed by these metals always lack the shell of nonmetal atom ligands and they always contain an interstitial atom in the octahedron center, an oxygen atom in alkali metal suboxides and a nitrogen atom in alkaline earth subnitrides. To the best approximation these are the ions O^{2-} and N^{3-}, respectively. This special bonding situation has unique consequences for the solid state. As these clusters or cluster condensates are ionic inside but metallic outside, crystals formed from them are metals with the peculiar property that conduction electrons are repelled by the static negative charges of the O^{2-} and N^{3-} anions. The term "void metal" applies to such systems. In the case of alkali metal suboxides it has been demonstrated that the confinement of conduction electrons to the intercluster regions results in quantum size effects [65] which reduce the work function of cesium (which is the lowest of all elements already) to slightly more than 1 $^{\prime}$ for $Cs_{11}O_3$ [5,9,10]. The effect is used in IR sensitive photocathodes.

The chemistry of alkali metal suboxides, their structure, bonding and properties have been described in great detail [5,9–12]. Recently, a very similar kind of chemistry emerged with subnitrides in the Ba–Na–N system.

Starting from early investigations on the reaction of nitrogen with barium dissolved in molten sodium [66], we were able to isolate crystals of $NaBa_3N$ [67], Na_5Ba_3N [68] and $Na_{16}Ba_6N$ [69] from such solutions. The structure of $Na_{16}Ba_6N$ represents a regular array of discrete Ba_6N clusters in sodium, and in the case of Na_5Ba_3N infinite chains of Ba_6N octahedra sharing opposite faces according to $Ba_{6/2}N = Ba_3N$ are inserted into a matrix of pure sodium. The structure is similar to that of $NaBa_3N$, which, due to the lower sodium content, also has inter-chain contacts. The structural principle is therefore entirely analogous to that of alkali metal suboxides, where Rb_9O_2 and $Cs_{11}O_3$ clusters formed by face-sharing of two and (cyclic) three M_6O octahedra, respectively, are bonded to the same or different alkali metals in compounds such as $Rb_9O_2Rb_3$, $Cs_{11}O_3Cs_{10}$ or $Cs_{11}O_3Rb_7$. In fact, the chemistry of barium subnitrides seems to offer an even broader range of structural variation, as the single M_6O cluster, the infinite chain and the layer, realized in Ba_2N (isotypic with Ca_2N [70,71]) are known. In that series with an increasing degree of condensation the Rb_9O_2 cluster takes the position of the first step of condensation towards the infinite chain; see Fig. 22.

The structure of Na_5Ba_3N is shown in Fig. 23. Recalling what has been said about the exclusion of conduction electrons from the regions of accummulated anionic charge, the compound represents a first realization of the inverse of a one-dimensional metal.

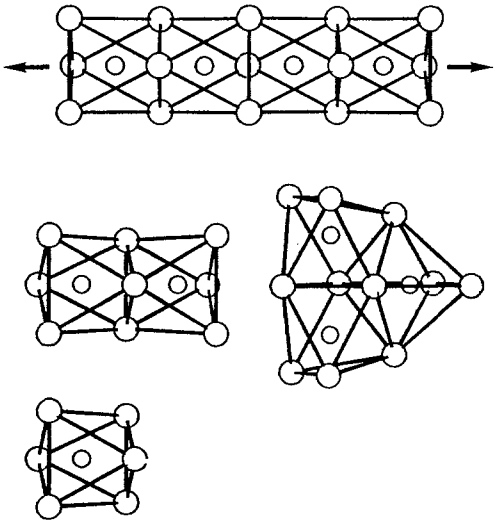

Fig. 22. Single M_6X units as found in $Na_{16}Ba_6N$, condensed units in the suboxide clusters Rb_9O_2 and $Cs_{11}O_3$ as well as in the infinite chain Ba_3N found in $NaBa_3N$ and Na_5Ba_3N.

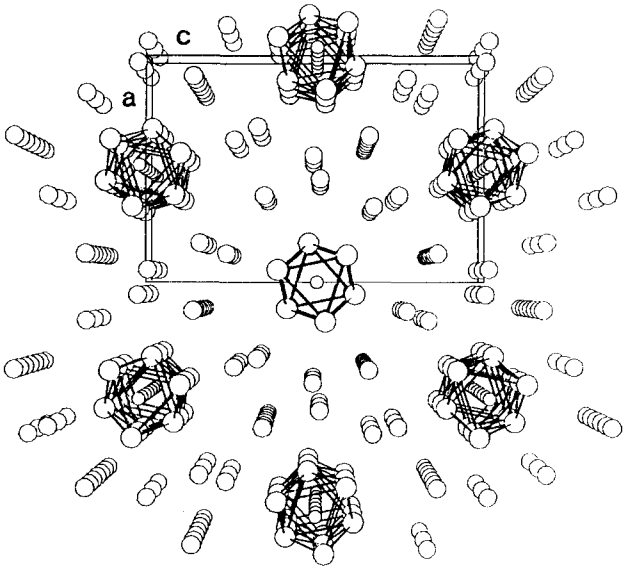

Fig. 23. Projection of the crystal structure of Na_5Ba_3N along [010] of the orthorhombic unit cell. The chains of face-sharing Ba_6N octahedra are outlined by bold lines; the unit cell is shown.

Instead of single metal atom chains surrounded by insulating ligands as e.g. in tetracyanoplatinates, here chains of N^{3-} anions are inserted into a metallic matrix. The special properties of such an "atomically drilled" metal still have to be elucidated.

3. Molecular crystals

In the introduction research was compared with a growing tree, and so far the stem comprising metal-rich compounds has been described. A number of branches grew from it, for example the Vegard type behavior found for topologically close-packed ordered intermetallic compounds [72, 73]. At the end one of the branches which has grown particularly large over the years will be described briefly.

The secret about alkali metal suboxides could only be uncovered with the help of specially designed apparatus equipment. An X-ray camera allowed investigations at continuously varied temperatures down to boiling nitrogen with the accuracy of the Guinier technique [74]. For single crystal investigations of the low-melting compounds in-situ crystal growth on diffractometers was performed with the help of a little apparatus [12,75]. We used these techniques frequently for the investigation of crystal structures and phase transitions of solidified gases and liquids, and a few examples of more general interest are described in the following.

3.1. Hydrogen bromide

The phase transitions in solid HBr had been chosen to demonstrate the experimental possibilities of the X-ray camera [74]. From previous very careful specific heat measurements it was known [76] that HBr undergoes three phase transitions, at 89.8, 113.6 and 116.7 K, respectively. Neutron diffraction experiments on DBr had revealed the structures of the low temperature modifications (III, II) [77], indicating a transition from order to two-fold disorder at 89.8 K. In our experiment it could be shown that the stable phase (Ib) in the 3.3 K interval between 113.6 and 116.9 K, which is only observed with HBr but not DBr, is cubic as the "high temperature" phase (Ia) above 116.9 K. The phase transition changed the lattice constant by less than 0.5%. The crystal structure of Ib determined by neutron diffraction many years later [78] is represented in Fig. 24. The bromine atoms occupy the positions of an fcc lattice, and the hydrogen atoms reorient in planes formed by six neighboring bromine atoms. The structure compares with that of CO_2 (or the sulfur sublattice in pyrite), the CO_2 molecule representing the axis of rotation for the hydrogen atom in HBr (Ib).

Hydrogen bromide is a beautiful example of a stepwise increase of (configurational) entropy in a solid from the ordered lattice at low temperature via a one-dimensional, followed by a two-dimensional and

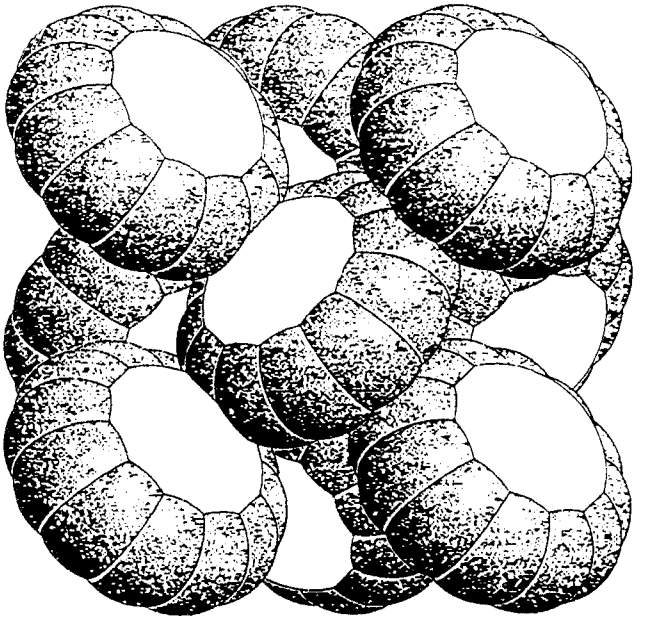

Fig. 24. Cubic crystal structure of HBr (Ib, 116 K). The planar disorder of the molecules is drawn with the van-der-Waals radii of Br and H.

finally ending in a three-dimensional disorder in the high-temperature form with randomly reorienting molecules. The group-theoretical formulation of the transformation pattern nicely explains the second order character of the Ia–Ib and II–III transitions, and the first order character which is already indicated experimentally by the pronounced hysteresis of the Ib–II transition.

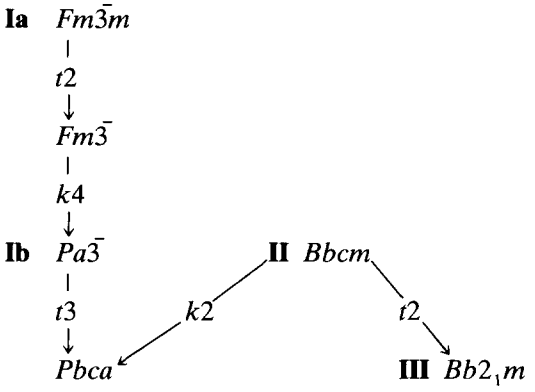

3.2. Dinitrogen trioxide

Fig. 25 shows a diagram of a prereacted N_2O_4–NO mixture taken with the previously mentioned X-ray camera [79]. The main lines are those of cubic N_2O_4 and N_2O_3, the latter exhibiting a complex pattern of phase transitions. Quenching experiments indicate further complications from the existence of hitherto unknown compound(s) between the compositional limits N_2O_3 and N_2O_4 [80]. The complexity of the system explains why earlier attempts to solve the crystal structure of N_2O_3 were unsuccessful [81].

A detailed knowledge of the phase relationships proved to be essential for successful crystal growth. On that basis single crystals of the (disordered) "high-temperature" phase (A) as well as the (ordered) phase B could be grown from the melt and their structures solved [79,80]. The structure of B–N_2O_3 is shown in Fig. 26. As proposed early on [82], N_2O_3 is a "nitroso-nitro" compound in the condensed state as in the gas phase. The comparison with the molecule in the gas phase [83] shows close agreement in all geometrical details, particularly with respect to the long distance

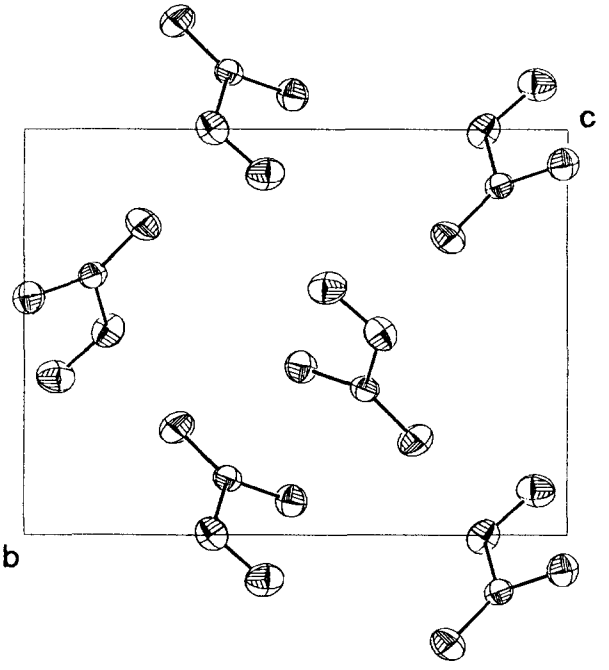

Fig. 26. Projection of the crystal structure of B–N_2O_3 at 110 K.

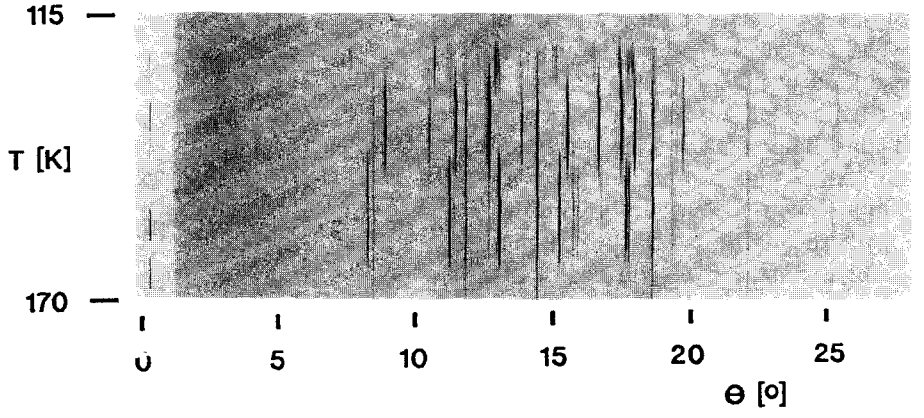

Fig. 25. Modified Guinier-type diagram of a N_2O_4 sample prereacted with NO and quenched to 100 K. At a heating rate of 1.3 K h^{-1} several reactions and phase transitions are observed. Top to bottom: amorphous sample, crystallization of an unknown phase together with diffuse lines of N_2O_4, transformation into well crystallized B–N_2O_3 + N_2O_4 followed by A–N_2O_3 + N_2O_4, melting of A–N_2O_3, only N_2O_4 persisting.

$d_{N-N} = 189.1$ pm in the crystal, which corresponds to a Pauling bond order near 0.2. In spite of this weak interaction the molecule is nearly planar, and packing effects in the solid do not change this characteristic feature of the gas phase species.

In order to complete our knowledge about nitrogen oxides the structures of metastable monoclinic and stable cubic N_2O_4 were reinvestigated [84] with a refinement of parameters; however, there were no surprises. However, N_2O_5 offers a surprise. The single crystal structure refines to $R = 0.028$ with linear NO_2^+ and planar NO_3^- ions in a hexagonal cell. Only Guinier-type powder diagrams indicate a marginal deformation by 0.3% of the (ortho-)hexagonal unit cell into an orthorhombic one. Why?

3.3. Nomenclature in N–O–Cl chemistry

Nitrosylchloride, NOCl, nitrylchloride, NO_2Cl and chlorine nitrate, NO_3Cl, attracted the early and recent interest of chemists, e.g., because NOCl is the essential component of aqua regia, and NO_3Cl is considered to play a role in ozone depletion in the stratosphere via the $ClO–NO_2$ reaction [85]. Crystal structures of these hazardous and low melting compounds (melting points are 212, 128 and 172 K for NOCl, NO_2Cl and NO_3Cl, respectively) were not known when we started our investigation [86]. Again, a prerequisite of the single crystal growth and structure determination was a detailed knowledge of phase relationships gained from continuous Guinier-type investigations. Single crystals of NOCl showed a transition at 142 K but could be cooled below the transition temperature and investigated at 113 K. No such complication occured with NO_2Cl and NO_3Cl. So crystals could be grown from the melts and measured at 103 K. The molecules as found in the crystals are depicted in Fig. 27.

The geometry of the NOCl molecule in the solid state is remarkably different to that in the gas phase [87], e.g. comparing $d_{N-Cl} = 217.3$ pm (solid) and $d_{N-Cl} = 197.5$ pm (gas). The relatively high melting point of NOCl provides evidence that significant changes occur upon condensation from the gas phase. Indeed, taking the N–O distance as a measure of the ionic character of the NO entity (115 and 106.3 pm for neutral NO and for the NO^+ cation, respectively) the partial charge increases from 0.12 + in the gas to 0.55 + in the solid.

A considerable degree of ionic bonding is found for solid NOCl, in marked contrast to NO_2Cl. The latter molecule is nearly planar like the isoelectronic NO_3^- ion. The mean distance $d_{N-Cl} = 182.5$ pm is much shorter than in NOCl and indicates largely covalent bonding, as does the almost identical shape of the NO_2 entity in NO_2Cl and N_2O_4. Whereas the name nitrosylchloride for NOCl is justified, the term nitrylchloride does not really apply to the covalent molecule NO_2Cl, whose slightly decreased O–N–O angle asks for a description in favor of $NO_2^{-\delta}$ rather than $NO_2^{+\delta}$. This trend is even enhanced for NO_3Cl, where the name chlorine nitrate is simply misleading. The molecular crystal contains planar NO_3 units, but with a large distance difference, $d_{N-O} = 147$ pm vs. 119 and 120 pm, respectively. Taking into account the distance $d_{Cl-O} = 168$ pm the formulation of NO_3Cl as an adduct of ClO and NO_2 with some small polarization towards $NO_2^{-\delta}$ seems the correct description for the compound.

One could go on with low-temperature structure determinations on textbook compounds such as Mn_2O_7 [88,89], Cl_2O_7 and $HClO_4$ [90], AsF_5 [91] and GeF_4 [92], just to mention a few out of many. Although the last was published in the *Journal of Less-Common Metals*, predecessor of the *Journal of Alloys and Compounds*, molecular crystals are somewhat remote from the main topics in the journal. Therefore, a last example is chosen to demonstrate the intimate link which might exist between molecular crystals and metals.

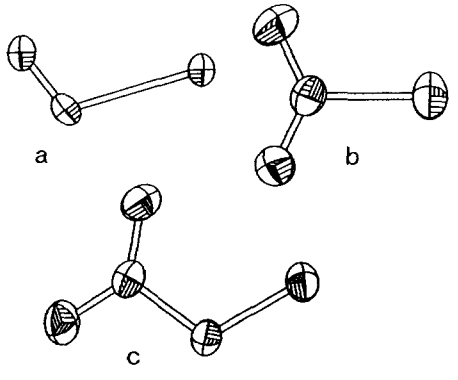

Fig. 27. Molecules in crystalline (a) NOCl, (b) NO_2Cl, and (c) NO_3Cl at approximately 110 K (assignment of atoms, see text).

3.4. White phosphorus, an analogue of metals

White phosphorus at ambient temperature and pressure has the complicated α-manganese structure, the Mn atoms being replaced by P_4 tetrahedra [93]. X-ray investigations of the plastic crystal revealed four subsets of P_4 molecules which exhibit different reorientational motions, and the scattering density of the phosphorus atoms is more or less smeared out on (structured) spheres [94]. A detailed analysis of the molecular geometries is made impossible by the disorder.

Under pressure, white phosphorus transforms into a second modification which becomes stable below 197

K [94]. Several early attempts to characterize this modification crystallographically had not succeeded [96–99].

In contrast to Ref. [93] but in agreement with Ref. [96], the low temperature modification is called β-phosphorus here, because quenching of the room temperature modification (α) to liquid nitrogen temperature and warming to 98 K results in another modification (γ) which transforms to β near 150 K [100]. As the transition is accompanied by an endothermic effect, the γ-form is the stable modification at still lower temperature than β. Nothing is known about the structure of the γ-form.

So far, no experimental details have been given in this overview article. At the end the crystal growing procedure for β-phosphorus [100,101] offers the chance of finally correcting this.

Fig. 28 shows the equipment used [75], which essentially consists of a heatable brass plate with a central bore that can be closed around the X-ray capillary and moved slowly up or down with the help of the threaded brass block attached to the goniometer head. The assembly is mounted in the diffractometer equipped with a cooling gas system. The entire apparatus is dismantled after crystal growth has finished without any interruption to the cooling of the sample. Normally, the tip of a capillary filled with the liquid sample reaches through the brass plate into the nitrogen stream set to appropriate temperatures, and crystal growth according to Bridgman is achieved by slowly lowering the brass plate in turning the φ-circle of the diffractometer. In the case of β-phosphorus the equipment is used differently.

The capillary is filled with a concentrated solution of phosphorus in CS_2 at room temperature. The entire length of the capillary is exposed to the nitrogen stream, the temperature of which is slowly decreased. Due to a miscibility gap the solution separates at 250 K into a phosphorus-rich phase collecting in the lower part and a dilute phase in the top part of the capillary. At a temperature of 193 K a few small crystallites of the β-form have grown from the very dilute solution. By raising the brass plate to approximately 1 mm below a selected crystallite in the top of the capillary, while keeping the top at 193 K, the concentrated phase is brought sufficiently near to the crystallite that within a few hours a large single crystal of β-phosphorus grows via small distance diffusion.

Fig. 29 shows the triclinic unit cell of β-phosphorus which contains well-ordered P_4 molecules. The packing is much more complicated than possible for tetrahedral molecules, which could be a close packing with respect to the atoms as in $SnBr_4$. Obviously, it is the size misfit between tetrahedral molecules and octahedral van-der-Waals voids and/or the presence of lone pairs at the phosphorus atoms interacting repulsively which leads to the complicated packing.

When analysing the molecular arrangement in β-phosphorus one finds that (as in α-phosphorus) the centers of the P_4 tetrahedra take the positions of yet another metal structure, that of γ-plutonium. This structure type is closely related to bcc, but with a rotation of successive atom layers by 60° when stacking them along [110] of the original bcc cell. Is it the 5f electron contribution in γ-plutonium that provokes this complicated stacking, and is this feature mimicked by the lone pairs of P_4? The structures of molecular crystals might help our understanding of the structures of metals and alloys and vice versa.

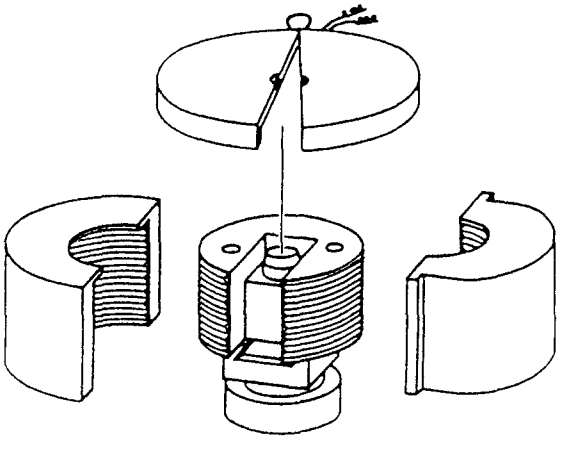

Fig. 28. Apparatus made of brass for in-situ crystal growth on a diffractometer.

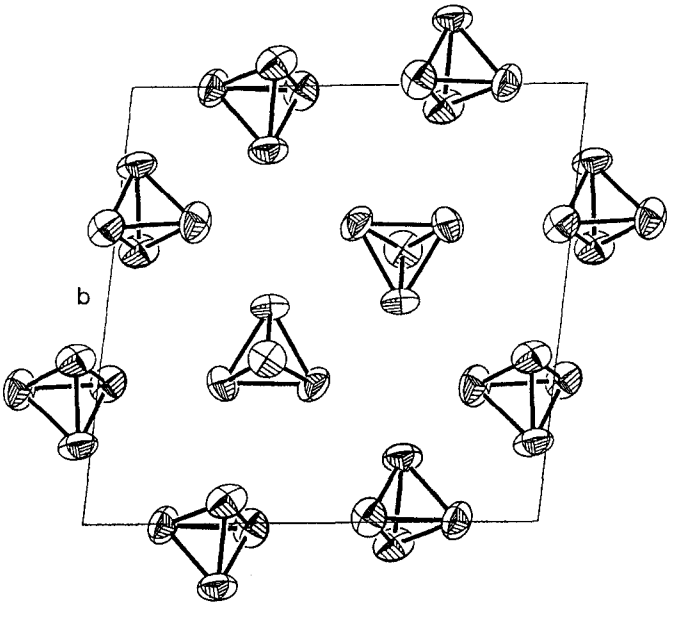

Fig. 29. Crystal structure of ordered white phosphorus (β-P_4, 160 K) projected along a of the triclinic unit cell.

References

[1] A. Simon, in G. Schmid (ed.), *Clusters and Colloids — From Theory to Applications*, Verlag Chemie, Weinheim, 1994, pp. 373.
[2] J. Köhler, G. Svensson and A. Simon, *Angew. Chem. Int. Ed. Engl., 31* (1992) 1437.
[3] A. Simon, in A.K. Cheetham and P. Day (eds.), *Solid State Chemistry — Compounds*, Clarendon Press, 1992, pp. 112.
[4] A. Simon, Hj. Mattausch, G. Miller, W. Bauhofer and R.K. Kremer in K.A. Gschneidner, Jr. and L. Eyring (eds.), *Handbook on the Physics and Chemistry of Rare Earths*, Vol. 15, North-Holland, Amsterdam, 1991, pp. 191.
[5] A. Simon, *Angew. Chem. Int. Ed. Engl., 27* (1988) 159 .
[6] A. Simon, *J. Solid State Chem., 57* (1985) 2.
[7] A. Simon, *Ann. Chim. France, 7* (1982) 539.
[8] A. Simon, *Angew. Chem. Int. Ed. Engl., 20* (1981) 1.
[9] A. Simon, *J. Solid State Chem., 27* (1979) 87.
[10] A. Simon, *Structure Bonding, 36* (1979) 81.
[11] A. Simon, in A.L. Rheingold (ed.), *Homoatomic Rings, Chains and Macromolecules of Main-Group Elements*, Elsevier Scientific, Amsterdam, 1977, pp. 117.
[12] A. Simon, in C.J.M. Rooymans and A. Rabenau (eds.), *Crystal Structure and Chemical Bonding in Inorganic Chemistry*, North-Holland, Amsterdam, 1975, pp. 47.
[13] D.G. Cooper, *The Periodic Table*, Butterworth & Co., London, 1968.
[14] A. Kjekshus and T. Rakke, *Structure Bonding, 19* (1974) 45.
[15] H.F. Franzen and J.G. Smeggil, *Acta Crystallogr. B, 25* (1969) 1736.
[16] F.A. Cotton and R.E. Haas, *Inorg. Chem., 3* (1964) 10.
[17] A. Simon, F. Böttcher and J.K. Cockcroft, *Angew. Chem. Int. Ed. Engl., 30* (1991) 101.
[18] F. Böttcher, A. Simon, R.K. Kremer, H. Buchkremer-Hermanns and J.K. Cockcroft, *Z. anorg. allg. Chem., 598/599* (1991) 55.
[19] T. Braun, Thesis, Stuttgart, 1994.
[20] S.J. Hibble, A.K. Cheetham, A.R.L. Bogle, H.R. Wakerley and D.E. Cox, *J. Am. Chem. Soc., 110* (1988) 3295.
[21] R. Dronskowski, A. Simon and W. Mertin, *Z. anorg. allg. Chem., 602* (1991) 49.
[22] C.C. Torardi and R.E. McCarley, *J. Am. Chem. Soc., 101* (1979) 3963.
[23] R.E. McCarley in J.P. Fackler, Jr. (ed.), *Metal-Metal Bonds and Clusters in Chemistry and Catalysis*, Plenum Press, New York, 1990, pp. 91.
[24] E. Fais, H. Borrmann, Hj. Mattausch and A. Simon, *Z. anorg. allg. Chem., 621* (1995) 1178.
[25] Hj. Mattausch, A. Simon and E.-M. Peters, *Inorg. Chem., 25* (1986) 3428.
[26] R. Dronskowski, Hj. Mattausch and A. Simon, *Z. anorg. allg. Chem., 619* (1993) 1397.
[27] R. Ramlau, E. Fais and A. Simon, to be published.
[28] A. Magnéli, *Chem. Scripta, 26* (1989) 535.
[29] G. Svensson, *Microsc. Microanal. Microstr., 1* (1990) 343.
[30] V.G. Zubkov, A.P. Tyutyunnik, V.A. Pereliaev, G.P. Shveikin, J. Köhler, R.K. Kremer, A. Simon and G. Svensson, *J. Alloys Comp.*, in press.
[31] B.O. Marinder, *Chem. Script., 11* (1977) 97.
[32] A. Simon, J. Köhler, R. Tischtau and G. Miller, *Angew. Chem. Int. Ed. Engl., 28* (1989) 1662.
[33] G. Svensson, J. Köhler and A. Simon, *Angew. Chem. Int. Ed. Engl., 31* (1992) 212.
[34] V.A. Gasparov, G.K. Strukova and S.S. Khassanov, *Pis'ma Zh. Eksp. Tear. Fiz., 60* (1994) 425.
[35] D.A. Lokken and D.J. Corbett, *Inorg. Chem., 12* (1973) 556.
[36] A. Simon, N. Holzer and Hj. Mattausch, *Z. anorg. allg. Chem., 456* (1979) 207.
[37] J.D. Corbett, *Inorg. Synth., 22* (1983) 15.
[38] G. Meyer and S. Uhrland, *Angew. Chem. Int. Ed. Engl., 32* (1993) 1318.
[39] M. Ruck and Simon, *norg. allg. Chem., 617* (1992) 7.
[40] G. Meyer, H. Mattfeld and K. Kraemer, *Z. anorg. allg. Chem., 619* (1993) 1384.
[41] Hj. Mattausch, H. Borrmann and A. Simon, *Z. Naturforsch., 48b* (1993) 1828.
[42] Hj. Mattausch, H. Borrmann, R. Eger, R.K. Kremer and A. Simon, *Z. anorg. allg. Chem., 620* (1994) 1889.
[43] Hj. Mattausch and A. Simon, *Angew. Chem.*, in press.
[44] C. Bauhofer, Hj. Mattausch, G.J. Miller, W. Bauhofer, R.K. Kremer and A. Simon, *J. Less-Common Met., 167* (1990) 65.
[45] W. Bauhofer and A. Simon, *Z. Naturforsch., 37a* (1982) 568.
[46] R.K. Kremer, K.U. Neumann and A. Simon, to be published.
[47] U. Schwanitz-Schüller and A. Simon, *Z. Naturforsch., 40b* (1985) 710.
[48] Hj. Mattausch, R.K. Kremer, R. Eger and A. Simon, *Z. anorg. allg. Chem., 609* (1992) 7.
[49] A. Simon, Hj. Mattausch, R. Eger and R.K. Kremer, *Angew. Chem. Int. Ed. Engl., 30* (1991) 1188.
[50] A. Simon, *Angew. Chem. Int. Ed. Engl., 26* (1987) 579.
[51] A. Bussmann-Holder, A. Simon and H. Büttner, *Phys. Rev. B, 39* (1989) 207. [52] H. Hentsch, N. Winzek, M. Mehring, Hj. Mattausch and A. Simon, *Physica C, 158* (1989) 137.
[53] L. Genzel, A. Wittlin, M. Bauer, M. Cardona, E. Schönherr and A. Simon, *Phys. Rev. B, 40* (1989) 2170.
[54] A. Bussmann-Holder, H. Büttner, A. Simon and V. Waas, *Z. Phys. B — Cond. Matter, 79* (1990) 445.
[55] J. Reedijk, *Bioinorganic Catalysis*, Marcel Dekker, New York, 1993.
[56] Proc. 30th Int. Conf. Coord. Chem., Kyoto, 1994, to appear in *Pure Appl. Chem., 67* (1995).
[57] C. Thomsen in U. Roessler (ed.), *Festkörperprobleme*, Vieweg, Braunschweig, 1991, p. 2.
[58] P.G. deGennes, *Superconductivity of Metals and Alloys*, Addison-Wesley, Reading, MA, 1989, p. 93.
[59] G.J. Miller, J.K. Burdett, C. Schwarz and A. Simon, *Inorg. Chem., 25* (1986) 4437.
[60] A. Simon, A. Yoshiasa, M. Bäcker, R. Henn, R.K. Kremer and Hj. Mattausch, *Z. Anorg. Allg. Chem.*, in press.
[61] M. Bäcker, *Diplomarbit*, Dusseldorf, 1994.
[62] B.W. Roberts, *J. Phys. Chem. Ref. Data, 5* (1976) 581.
[63] A. Simon, J.G. Smith and R.K. Kremer, unpublished.
[64] B. Matthias, *Phys. Rev., 97* (1955) 74.
[65] M.G. Burt and V. Heine, *J. Phys. C, 11* (1978) 691.
[66] C.C. Addison, R.J. Pulham and E.A. Trevillion, *J. Chem. Soc. Dalton Trans.* (1975) 2080.
[67] P.E. Rauch and A. Simon, *Angew. Chem. Int. Ed. Engl., 31* (1992) 1519.
[68] G.J. Snyder and A. Simon, *J. Am. Chem. Soc., 117* (1995) 1996.
[69] G.J. Snyder and A. Simon, *Angew. Chem. Int. Ed. Engl., 33* (1994) 689.
[70] T. Künzel, Thesis, Stuttgart, 1980.
[71] E.T. Keve and A.C. Skapski, *Inorg. Chem., 7* (1968) 1757.
[72] A. Simon, *Angew. Chem. Int. Ed. Engl., 22* (1981) 95.
[73] G.J. Snyder and A. Simon, *Z. Naturforsch., 49b* (1994) 189.
[74] A. Simon, *J. Appl. Crystallogr., 4* (1971) 138.
[75] A. Simon, H.-J. Deiseroth, E. Westerbeck and B. Hillenkötter, *Z. anorg. allg. Chem., 423* (1976) 203.
[76] W.F. Giauque and R. Wiebe, *J. Am. Chem. Soc., 50* (1928) 2193.
[77] E. Sándor and M.W. Johnson, *Nature, 217* (1968) 541.
[78] J.K. Cockcroft, A. Simon and K.R.A. Ziebeck, *Z. Kristallogr., 184* (1988) 229.

[79] J. Horakh, H. Borrmann and A. Simon, *Chem. Eur. J.*, submitted.
[80] A. Simon, J. Horakh, A. Obermeyer and H. Borrmann, *Angew. Chem. Int. Ed. Engl., 31* (1992) 301.
[81] T.B. Reed and W.N. Lipscomb, *Acta Crystallogr., 6* (1953) 781.
[82] H. Wieland, *Berichte, 54* (1921) 1781.
[83] A.H. Brittain, A.P. Cox and R.L. Kuczkovski, *Trans. Faraday Soc., 65* (1969) 1963.
[84] A. Obermeyer, H. Borrmann and A. Simon, *Z. Kristallogr., 196* (1991) 129.
[85] M.R.S. McCoustra and A.B. Horn, *Chem. Soc. Rev.* (1994) 195.
[86] A. Obermeyer, H. Borrmann and A. Simon, *J. Am. Chem. Soc.*, submitted.
[87] D.J. Millen and J. Panel, *J. Chem. Soc.*, (1961) 1322.
[88] A. Simon, R. Dronskowski, B. Krebs and B. Hettich, *Angew. Chem. Int. Ed. Engl., 26* (1987) 139.
[89] R. Dronskowski, B. Krebs, A. Simon, G. Miller and B. Hettich, *Z. anorg. allg. Chem., 558* (1988) 7.
[90] A. Simon and H. Borrmann, *Angew. Chem. Int. Ed. Engl., 27* (1988) 1339.
[91] J. Köhler, A. Simon and R. Hoppe, *Z. anorg. allg. Chem., 575* (1989) 55.
[92] J. Köhler, A. Simon and R. Hoppe, *J. Less-Common Met., 137* (1988) 333.
[93] J. Donohue, *The Structures of the Elements*, John Wiley & Sons, New York, 1974, p. 298.
[94] H.G. v. Schnering, *Angew. Chem. Int. Ed. Engl., 20* (1981) 33.
[95] P.W. Bridgman, *J. Am. Chem. Soc., 36* (1914) 1344.
[96] G. Natta and L. Passerini, *Nature, 125* (1930) 707.
[97] G. Natta and L. Passerini, *Atti Accad. Naz. Lincei, Classe Sci. Fis., Mat. Nat., 24* (1936) 464.
[98] T. Sugawara, Y. Sakamoto and E. Kanda, *Sci. Rep. Res. Inst. Tohoku Univ., 1* (1949) 29.
[99] T. Sugawara and E. Kanda, *Sci. Rep. Res. Inst. Tohoku Univ., 1* (1949) 153.
[100] H. Borrmann, Thesis, Stuttgart, 1988.
[101] A. Simon, H. Borrmann and H. Craubner, *Phosphorus Sulfur, 30* (1987) 507.
[102] W.A. Zachariasen and F.H. Ellinger, *Acta Crystallogr., 8* (1955) 431.